AVEIRO - PORTUGAL

Please cite this article as: Brites, C.D.S., Kuznetsov, S.V., Konyushkin, V.A., Nakladov, A.N., Fedorov, P.P. and Carlos, L.D. (2020), Simultaneous Measurement of the Emission Quantum Yield and Local Temperature: The Illustrative Example of SrF_2:Yb^{3+}/Er^{3+} Single Crystals. Eur. J. Inorg. Chem., 2020: 1555-1561. doi:10.1002/ejic.202000113

Simultaneous measurement of the emission quantum yield and local temperature: the illustrative example of SrF_2:Yb^{3+}/Er^{3+} single crystals

Carlos D.S. Brites,*[a] Sergey V. Kuznetsov,[b] Vasilii A. Konyushkin,[b] Andrey N. Nakladov,[b] Pavel P. Fedorov,[b] and Luís D. Carlos [a]

[a] Prof. C.D.S. Brites, Prof. L.D. Carlos
Phantom-g, CICECO – Aveiro Institute of Materials, Department of Physics
Universidade de Aveiro
3810-193 Aveiro, Portugal
E-mail: carlos.brites@ua.pt, http://hybrids.web.ua.pt/CDSBrites.html

[b] Dr. S.V. Kuznetsov Dr. V.A. Konyushkin, Dr. A.N. Naklavov, Prof. P.P. Fedorov
Prokhorov General Physics Institute of the Russian Academy of Sciences
119991, Moscow, Russia

Supporting information for this article is given via a link at the end of the document.

Abstract: The emission quantum yield is one of the key figures of merit to evaluate the photoluminescence performance of luminescent materials. The emission quantum yield of upconverting materials is still not widely reported due to technical difficulties and intricate dependence on the excitation power density that is mirrored in a temperature increase. This work describes the simultaneous determination of the emission quantum yield (for both downshifting and upconverting processes) and of the temperature using the output of a commercial integrating sphere. The temperature is calculated by primary luminescence thermometry through the Boltzmann equation, analyzing the intensity ratio between the $^2H_{11/2}$, $^4S_{3/2}\rightarrow{}^4I_{15/2}$ transitions. The procedure is illustrated using of SrF_2: Yb^{3+}/Er^{3+} single crystals with distinct Yb^{3+} compositions and the effect of the Yb^{3+} content in the emission quantum yield and in temperature increase of the sample.

Introduction

Absolute quantum yield is a central figure of merit of luminescent materials, allowing the direct comparison of the emission features of distinct materials irrespectively of their nature.[1-3] This is a crucial variable for methodical performance evaluation and comparison of luminescent materials.[4] It is defined as the number of emitted photons per absorbed photon, directly measuring the efficiency of the conversion of absorbed into emitted photons.[4-5] The well-known excitation power density dependence of the emission quantum yield of upconverting materials requires its measurement as a function of the excitation power density.[6] It is established that the comparison of the performance of upconverting phosphors should be made on the saturation regime, corresponding to the maximum emission quantum yield value.[7] However, the high excitation power density required for luminescence saturation can eventually lead to a substantial increase in temperature[8] that is still, as far as we know, not studied.

One of the upconverting materials most auspicious applications is nanothermometry, aiming to measure the temperature with excellent accuracy in nano- and submicron-sized scale using the emission of the material.[9-12] The ratiometric sensing based on lanthanide-based materials is a well-known and broadly reported technique for applications in theranostics[13-15] or catalysis,[16] for instance. Moreover, for the particular case of upconverting materials based on Yb^{3+}/Er^{3+}, some of us have reported that these materials are intrinsically primary luminescent thermometers.[17-20] The Boltzmann equation univocally relates the relative population of the $^4S_{3/2}$ and $^2H_{11/2}$ states of Er^{3+} with the temperature, circumventing the requirement of performing the previous calibration of the materials.[20]

The upconverting emission quantum yield was studied for several trivalent lanthanide (Ln^{3+}) ions but the most studied are Yb^{3+}/Er^{3+} co-doped materials, exhibiting a notorious non-linearity with the excitation power density (P_D) in distinct host materials.[2-3, 21-23] Strontium fluoride host crystals co-doped with ytterbium and erbium (SrF_2: Yb^{3+},Er^{3+}) are attractive materials due to their high up-conversion quantum yield. This is an atypical phenomenon for substances with a highly symmetric cubic face-centered lattice, despite it is consistently proved in the literature that the Ln^{3+} ions form $[Ln_6F_{37}]^{19-}$ clusters that easily substitute clusters $[Sr_6F_{32}]^{20-}$ in the crystal structure of the SrF_2.[24-25]

The synthesis of nano- and submicrometric-sized powders of SrF_2 doped with rare-earth elements for different applications is well known.[26-35] It is recognized that powders present a large specific surface area, leading to changes in the absorption and reflection properties of the material in comparison with those of a single-crystal sample. All these particular features of each sample preclude the direct comparison of the emission properties of materials even when they are based on the same host and have the same doping ions. Maybe the wisest practical approach for comparing the photoluminescent figures of merit of distinct materials is to use a reference sample with a well-established crystal structure and chemical composition. In this context, single-crystal samples are advantageous as they are ideal classical crystalline objects, mitigating numerous problems associated with the surface of the powders.

In the past, some of us observe a temperature increase induced by the irradiation of SrF_2: Yb^{3+}/Er^{3+} nanoparticles with a 980 nm laser with power density values up to ~10^3 $W{\cdot}cm^{-2}$, and we concluded that the excitation power density and the temperature increase cannot be decoupled.[21] On another work, some of us described the implementation of a simple and cost-

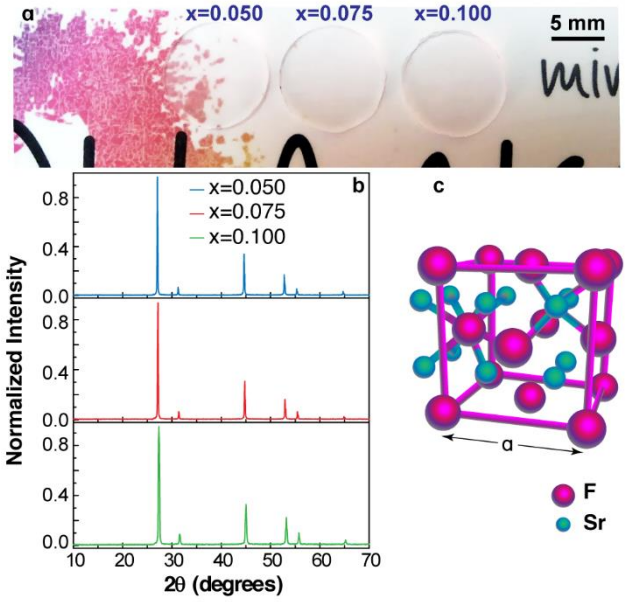

Figure 1. (a) Photograph of the $Sr_{1-x}Yb_xEr_{0.015}F_{2.015+x}$ (x=0.050, 0.075, 0.100) single crystals under daylight illumination. **(b)** X-ray powder diffraction of the single crystals **(c)** Crystal structure of the SrF_2 in the fluorite phase.

effective quantum-yield measurement setup using a commercial integrating sphere-based spectrometer operating in the visible spectral range and a power meter to determine the incident number of photons,[21] calculating the upconverting quantum yield. Its dependence on the excitation power density for SrF_2: Yb^{3+}/Er^{3+} nanoparticles in powder and water suspension was reported, however, until now it is lacking any method permitting the simultaneous determination of the emission quantum yield and of the temperature using a single experimental assessment.

Here, we used the spectral power density spectrum recorded by a commercial integrated sphere to calculate simultaneously the absolute quantum yield - both in visible and near-infrared (NIR) ranges - and the absolute temperature of SrF_2: Yb^{3+}/Er^{3+} crystals as a function of the irradiating laser power density. The results obtained for distinct Yb^{3+} compositions (5.0, 7.5 and 10.0 mol %) are compared and the dependence of the emission quantum yield with the excitation-induced temperature increase is presented for the first time. We also correlate the Yb^{3+} concentration with the maximum temperature increase and with the downshifting and upconverting quantum yield.

Results and Discussion

Structural Characterization

A series of high optical quality single crystals (Figure 1a) of $Sr_{1-x}Yb_xEr_{0.015}F_{2.015+x}$ (x=0.050, 0.075, 0.100) solid solution were grown. The photos of the polishing samples demonstrated the high optical quality of growing single crystals without any inclusions and inhomogeneity.

The crystalline phase of the samples was determined using X-ray powder diffraction (Figure 1b), that revealed the fluorite-type single-phase depicted in (Figure 1c). The face-centered cubic cell with fluorite structure characterized by ordered atom positions. The unit cell parameters of $Sr_{1-x}Yb_xEr_{0.015}F_{2.015+x}$, with x=0.050, 0.075, 0.100, solid solutions are 5.750(4) Å, 5.735(5) Å, and 5.709(6) Å, repectivelly. We notice that the calculated unit cell parameters differ from unit cell parameters for pure strontium fluoride *a* = 5.800 Å, respectivelly (JCPDS 06-0262). This is due to the solid solution formation as interstitial fluorine ions[36] and smaller ionic radii of the rare earth dopants (compared with strontium ion[37]) are added to the crystal.

Downshifting and Upconverting Quantum Yield

Upon 980 nm irradiation, all the tested samples present strong emission both in the visible and in the NIR spectral ranges. An illustrative emission spectrum of the samples $Sr_{1-x}Yb_xEr_{0.015}F_{2.015+x}$ is presented in Figure 2a for *x*=0.050 (the spectra for *x*=0.075 and *x*=0.100 are presented in Figure S1 in Supporting Information). The spectrum is dominated by the $^4F_{9/2}\rightarrow{}^4I_{15/2}$ transition in the red spectral range however the $^2H_{11/2}$, $^4S_{3/2}\rightarrow{}^4I_{15/2}$ ones are perfectly observed out of the noise level. The $^4I_{11/2}$, $^4I_{13/2}\rightarrow{}^4I_{15/2}$ transitions in the NIR spectral range are also observed.

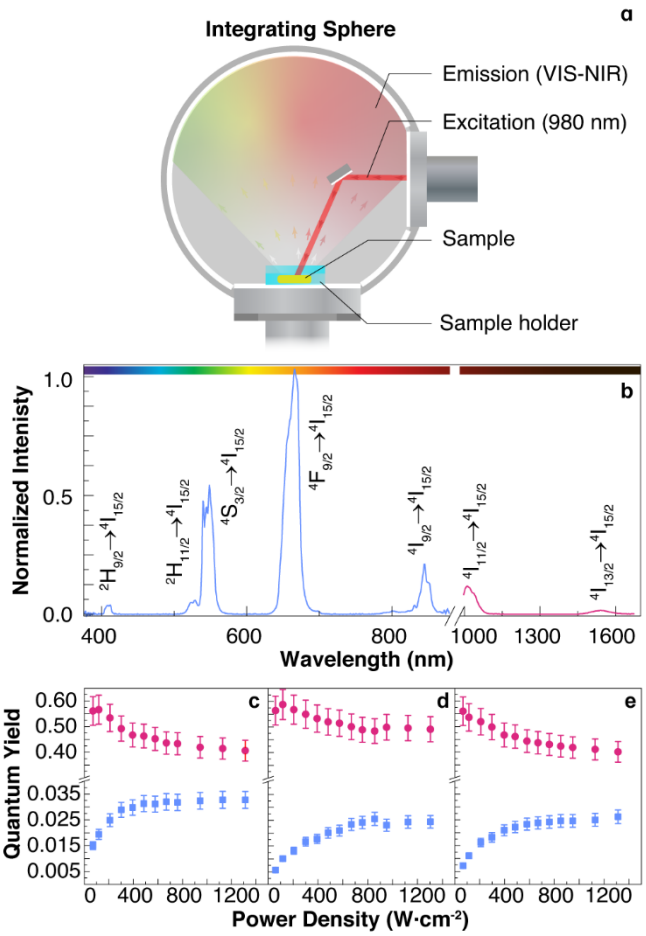

Figure 2. (a) Schematic of the integrating sphere setup used for determination of the quantum yield **(b)** Room-temperature emission spectra of $Sr_{0.95}Yb_{0.05}Er_{0.015}F_{2.065}$ under 980 nm excitation (P_D = 301 W·cm^{-2}). The Er^{3+} transitions in the visible and NIR spectral ranges are signed. The comparison of the emission intensity in both spectral ranges is not possible because two distinct detectors were used. Emission quantum yield for distinct excitation power density values (P_D) of $Sr_{1-x}Yb_xEr_{0.015}F_{2.015+x}$, with **(c)** x=0.050, **(d)** x=0.075, and **(e)** x=0.100. In (b), (c) and (d) the red circles and the green squares represent the downshifting and upconverting quantum yield, respectively.

To evaluate the effect of the irradiation power density on the temperature and on the quantum yield of the samples we scan the 70 –1300 W·cm^{-2} power density range. The upconverting quantum yield values correspond to the integration performed by the equipment in the visible spectral range (400-700 nm) and the

downshifting ones to the integration in the NIR spectral range (1000 -1650 nm). All the details of the determination of the emission quantum yield values are presented in the Experimental Section.

The dependence of the emission quantum yield with the 980 nm excitation power density is presented in Figure 2b-d for $Sr_{1-x}Yb_xEr_{0.015}F_{2.015+x}$ (x=0.050, 0.075, 0.100) solid solutions. As P_D increases, we observe the systematic decrease of the downshifting quantum yield and the simultaneous increase of the upconverting quantum yield. The sum of the up-conversion and downshifting quantum yield decrease as the laser power density increases.

The values obtained here are comparable to those reported by some of us for up-conversion quantum yields of SrF_2: Yb^{3+},Er^{3+} sub-micron particles prepared by precipitation from aqueous solution.[24] In the past, it was observed this characteristic increase of the upconverting emission quantum yield with the increase of the excitation laser power density, leading to a constant value between 0.02 and 0.03 depending on the Yb^{3+} content, that is in line with the results presented here. To the best of our knowledge, the downshifting quantum yield in the NIR spectral range was not found in the literature for this host.

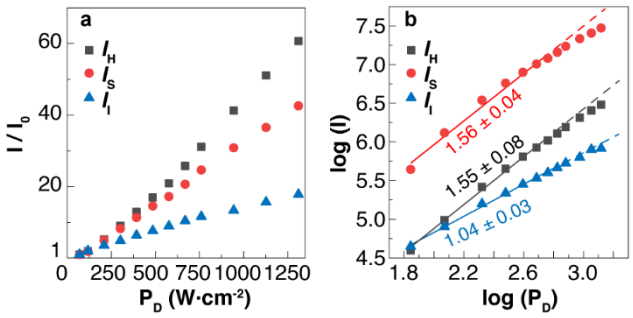

Figure 3. (a) Laser power density dependence of the integrated areas of $^2H_{11/2}\rightarrow{}^4I_{15/2}$ (I_H), $^4S_{3/2}\rightarrow{}^4I_{15/2}$ (I_S) and $^4I_{13/2}\rightarrow{}^4I_{15/2}$ (I_I) transitions, normalized to I_0, the value at the lowest power density value (70 W·cm^{-2}), illustrated for sample $Sr_{0.95}Yb_{0.05}Er_{0.015}F_{2.065}$ (results of other samples are presented in Supporting Information) **(b)** Double-logarithmic plot of the excitation power with the integrated areas I_H, I_S and I_I. The lines are the best linear regression with the slope values presented (r^2>0.98).

Simultaneous quantum yield and temperature determination

In this section, we describe the processing of the spectral photon flux density recorded by the quantum yield system to obtain the temperature of the sample. All the data exported from the equipment were post-processed in MatLab®. The reference signal is first subtracted to the sample signal and then the integrated area of the $^2H_{11/2}\rightarrow{}^4I_{15/2}$ (500-533 nm range), $^4S_{3/2}\rightarrow{}^4I_{15/2}$ (533-575 nm range) and $^4I_{13/2}\rightarrow{}^4I_{15/2}$ (620-705 nm range) Er^{3+} transitions (denoted hereafter by I_H and I_S, respectively) are calculated. The areas correspond to the integration of the spectral photon flux density exported from the quantum yield system (in units of photons per unit of time and per wavelength unit) and thus are expressed as photon flux (in units of photons per unit time).

Figure 3a presents the 980 nm laser power density dependence of I_H, I_S and I_I. As the excitation power density increases I_H, I_S and I_I increase 60, 40 and 17 times relative to the values measured at the lowest power density (Figure 3a), for a power density increased by 18 times. All the integrated areas follow a power law, i.e. $I \propto P_D^n$ (n is the number of photons involved in the process). The slope of the log-log plot (Figure 3b) reveals a number of photons around 1.5 for both I_H and I_S in line with the two-photon up-converting process. On the other hand, the downshifting transitions follow a one-photon process with n ~1, as expected.

The absolute temperature can be determined using the I_H and I_S integrated areas transitions as recurrently described in the literature.[13] Defining the thermometric parameter as $\Delta = I_H/I_S$, the temperature (T) can be calculated through:

$$\frac{1}{T} = \frac{1}{T_0} - \frac{k_B}{\Delta E}\ln\left(\frac{\Delta}{\Delta_0}\right) \qquad (1)$$

where T_0 corresponds to the temperature in the limit of null laser-induced heating (the room temperature), k_B is the Boltzmann constant, ΔE is the energy difference between the barycenter of the thermally coupled energetic levels, and Δ_0 is the thermometric parameter in the limit $P_D \rightarrow 0$ (and thus $T \rightarrow T_0$).

Table 1. Summary of the ΔE and Δ_0 parameters for the $Sr_{1-x}Yb_xEr_{0.015}F_{2.015+x}$ samples. The dependence of Δ with the power density (used to calculate Δ_0) and the deconvolution of the emission spectra are presented in Figures S1 and S2, respectively.

x	ΔE (cm^{-1})	Δ_0	T_0 (K)
0.050	735±20	0.0705 ± 0.0002	300
0.075	723±20	0.0708 ± 0.0008	300
0.100	693±20	0.0670 ± 0.0002	300

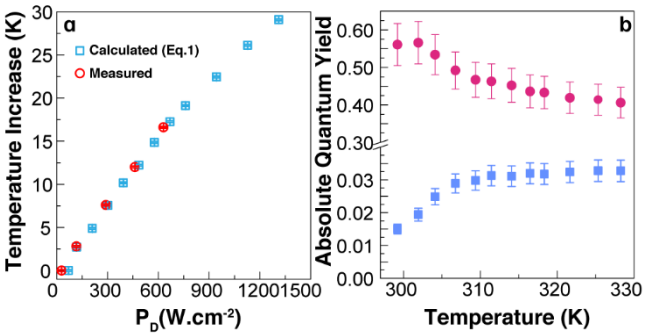

Figure 4. (a) Temperature increase in $Sr_{0.95}Yb_{0.05}Er_{0.015}F_{2.065}$ with the irradiating 980 nm laser power density. The calculated and measured temperatures are obtained using Eq. 1 and determined by a K-type thermocouple in direct contact with the crystal. **(b)** Temperature dependence of the absolute emission quantum yield for the downshifting (squares) and upconverting (circles) transitions.

We stress that all the parameters in Eq. 1 can be easily calculated from the experimental data collected from the quantum yield setup system. Details of the determination of ΔE and Δ_0 are given in the Experimental Section, yielding the values listed in Table 1. In general, ΔE and Δ_0 values are similar for the samples with lower Yb^{3+}content decreasing for the sample with higher concentration.

For all the samples studied we observe a linear increase of Δ with the increase of the laser power density for values below 750 W ·cm^{-2} and an increase with a lower slope for higher P_D values. The spectral photon density recorded by the quantum yield integrating sphere setup was converted in absolute temperature through Eq. 1. Figure 4 presents the temperature increase for $Sr_{0.95}Yb_{0.05}Er_{0.015}F_{2.065}$, as an illustrative example (the

measurements for the other single crystal compostions are given in Figures S2 and S3 in Supporting Information).

In Figure 4a we observe a good agreement between the temperature increase calculated using Eq. 1 and the values recorded by a thermocouple in contact with $Sr_{0.95}Yb_{0.05}Er_{0.015}F_{2.065}$, attesting the validity of this equation to predict the temperature increase induced by the 980 nm laser irradiation (the corresponding curves for the other single crystal compostions are presented in Figures S4 and S5 in Supporting Information). As stressed in previous works of some of us, luminescent thermometers based on the intensity ratio of transitions originated in thermally coupled levels (such as the well-known case of Er^{3+}-based systems) are intrinsically primary thermometers, and thus the calibration curve can be determined *a-priori*.

The temperature dependence of the emission quantum yield presented in Figure 4b can be easily calculated from the relation between the excitation power density and the temperature. We observe, in good agreement with the few results presented in the literature, the decrease of the emission quantum yield of the transitions due to the downshifting energy transfer. To the best of our knowledge, the emission quantum yield was not reported as a function of the temperature for the transitions arising from the upconverting energy transfer processes. As the temperature increase follows the excitation power density, we observe a constant value of the emission quantum yield for the upconverting processes, in all the samples in the power density range tested here.

Figure 5 presents the emission quantum yield of the distinct samples upon the maximum 1300 $W{\cdot}cm^{-2}$ excitation power density. The 980 nm laser irradiation induces a temperature increment around 30 K in the single crystals, observing temperature increases between 29.0 and 31.8 K. Comparing the distinct $Sr_{1-x}Yb_xEr_{0.015}F_{2.015+x}$ samples temperature increase we observe a smooth increase of 0.4 K between x=0.050 and x=0.075 and a 2.7 K increase between x=0.050 and x=0.100. Thus, we conclude that the higher Yb^{3+} content led to a higher temperature increase. This is in agreement with the most probably Yb→Yb energy transfers for the higher Yb^{3+} concentration that outcomes as energy dissipation in the single crystal that is released as heat.

Evaluating the dependence of the emission quantum yield at maximum excitation power density with the resultant temperature increase we observe symmetrical trends in the downshifting and on the upconverting transitions. The emission quantum yield under maximum excitation power density (and thus maximum temperature increase) for the transitions in the NIR spectral range slight increase within the uncertainty of the measurement between x=0.050 and x=0.075 and decrease between x=0.075 and x=0.100, still within the measurement uncertainty. For the transitions in the visible spectral range (originated by a two-photon upconverting process) the trend is basically the opposite, decreasing between x=0.050 and x=0.075 and increasing between x=0.075 and x=0.100. In the upconverting transitions, the changes are out of the experimental uncertainty. We recall that the exact same symmetry on the trends of the downshifting and upconverting transitions was observed when the laser power density was increased. These results suggest that as the temperature increase, we observe a quench in the downshifting emission quantum yield that is ascribed to the increasing deactivation mechanisms that are thermally enhanced.

As far as we know, there are no systematic studies on the temperature dependence of the upconverting quantum yield. Even the temperature dependence of the downshifting processes is scarcely reported. The quantum yield of $[Ru(bpy)_3]^{2+}$ was reported by Ishida *et al.* in acetonitrile and water.[38] The authors observed that the emission quantum yield of the downshifting transition is strongly temperature-quenched and attributed it to the non-radiative processes that are favored with the upon heating. Additionally, changing the solvent used the temperature dependence of the emission quantum yield also changes.

Our results suggest that in the tested samples and for the laser power density range covered, a portion of the absorbed photons at 980 nm is upconverted with enhanced efficacy as the laser power density increases. On the contrary, the temperature increase resulting from the excitation laser irradiation quenches the upconverting process. Thus, the typical non-linear dependence of the emission upconverting quantum yield is a balance between the enhancement due to higher excitation photons available and quenching due to non-radiative processes that are favored with the upon heating. The usually reported upconverting emission quantum yield on saturated absorption (higher power density values) is here explicitly correlated with the increase of the temperature of the nanocrystal.

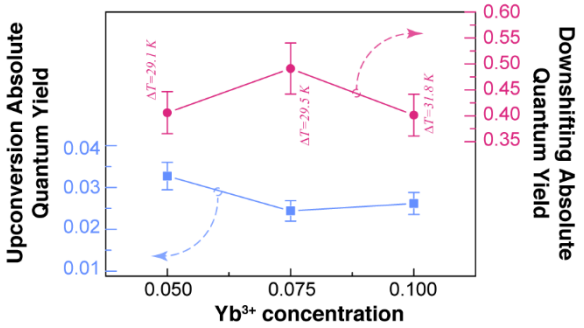

Figure 5. Dependence of the emission quantum yield of the upconverting (squares) and downshifting (circles) transitions with the Yb^{3+} concentration in **1-3.** The temperature increase values (ΔT) are presented.

Conclusions

Emission quantum yield is recognized as one important tool to compare the emission properties of luminescent materials. With the increasing attention being given to upconverting materials based on Ln^{3+} ions, the accurate determination and comparison of its emission quantum yield becomes imperative. Contrary to the emission quantum yield of downshifting transitions that typically are excitable with low excitation power densities (< 1$W{\cdot}cm^{-2}$) and are not expected to display a dependence on the excitation power density, upconverting materials are very commonly excited using high excitation power densities (> 1000 $W{\cdot}cm^{-2}$), presenting a non-linear increase of the emission quantum yield until reaching a saturation regime. Until now in the literature was suggesting that such high-power densities can induce significant temperature increase, however, it was not quantified.

In this work, we demonstrate that it is possible to calculate simultaneously the emission quantum yield and to estimate the temperature increase using a commercial setup and the emission lines of the Ln^{3+} ions. Luminescence primary thermometry was here used to demonstrate that is impossible to decouple the increase in the power density of the 980 nm CW laser excitation from the temperature increase. For the SrF_2 single crystals co-doped with Yb^{3+} and Er^{3+} studied here, that temperature increase

is clearly non-negligible and can be higher than 30 K, depending on the laser power density.

Using the current commercial setup, it is not possible to increase the excitation power density without changing the temperature of the sample. In the near future, we will address the precise control of the temperature that will permit us to quantify the effect of the temperature increase on the upconverting and downshifting quantum yields, upon constant excitation power density.

Experimental

Materials and Synthesis

Fluoride single crystals. The growing of fluoride single crystals with high optical quality is a very complicated task due to fluorides undergo pyrohydrolysis. The strontium fluoride, ytterbium fluoride, and erbium fluoride were 99.99 % (LANHIT, Russia). Each fluoride precursor was preliminarily melted in a vacuum with the CF_4 fluorinating atmosphere for eliminated oxygen impurities as humidity. The fluoride single crystals were grown by the Bridgman technique in a vacuum furnace with CF_4 fluorinating atmosphere. The graphite heater with a temperature gradient (60 $K \cdot cm^{-1}$) was used. The crucible was made of graphite because fluorides do not react with graphite. The crystallization temperature was chosen based on the SrF_2-ReF_3 phase diagrams.[39] The crystallization rate (6 mm $hour^{-1}$) was estimated based on the stability function.[40] Finally, a series of single crystals without cellular substructure with high optical quality of $Sr_{1-x}Yb_xEr_{0.015}F_{2.015+x}$ (x=0.050, 0.075, 0.100) solid solution with the fluorite structure were grown.

X-ray characterization. The single crystals were ground in an agate mortar up to micron-size grains. X-ray powder diffraction was carried out on Bruker D2 Phaser with CuK_α radiation. The unit cell parameters were calculated by Powder 2.0 software with ΔQ error of less than 10.

Emission Quantum Yield. The absolute emission quantum yields were measured without external temperature control using a quantum yield measurement system C13534 from Hamamatsu with a 150 W Xenon lamp coupled to a monochromator for wavelength discrimination, an integrating sphere as sample chamber and two multi-channel analyzers for signal detection in the visible and in the NIR ranges. For 980 nm excitation, an external laser diode (FC-980-5W, CNI Lasers) was used. The laser power can be adjusted between 0 and 5 W controlling the laser diode current. The illumination area in the sample holder is 0.0025 cm^2 accordingly to the manufacturer. Three measurements were made for each sample and the average is reported. The method is accurate within 10%.

This equipment measured the absolute quantum yield using the reference spectral power density, recorded with an empty sample holder, and the sample spectral power density, obtained in the same experimental conditions but in the presence of the sample. The equipment's software computes the emission quantum yield using the wavelength integration ranges for excitation and emission. We export the recorded signal as photon flux and post-process it in MatLab for baseline (photon flux of the reference signal) removal for further absolute temperature determination, as detailed in the next section.

Primary thermometry. The energy difference ΔE between the barycentres of the $^2H_{11/2}$ and $^4S_{3/2}$ levels was estimated from the high spectral resolution using the up-conversion emission spectra measured in the quantum yield measurement system. From the emission spectra, the ΔE was inferred by fitting the envelope of the $^2H_{11/2} \rightarrow {}^4I_{15/2}$ and $^4S_{13/2} \rightarrow {}^4I_{15/2}$ transitions using Gaussian functions. The barycenter of the $^2H_{11/2}$ and of the $^4S_{13/2}$ levels were calculated by a weighted arithmetic mean using the fitted area and peak energy of each Gaussian function. The energy gap ΔE was the difference between the barycentres of the transitions. The Δ_0 value was calculated taking the power density dependence of Δ and fitting a straight line to the experimental data before reaching the saturation regime (P_D<600 $W \cdot cm^{-2}$). The intercept of the straight line is taken as Δ_0. The ΔE and Δ_0 parameters for each sample were used in Eq. 1 to calculate the absolute temperature.

Acknowledgements

This work was developed within the scope of the project CICECO-Aveiro Institute of Materials, UIDB/50011/2020 & UIDP/50011/2020, financed by national funds through the FCT/MEC and when appropriate co-financed by FEDER under the PT2020 Partnership Agreement. This work was financially supported by the project (NanoHeatControl, POCI-01-0145-FEDER-031469), funded by FEDER, through POCI and by national funds (OE), through FCT/MCTES. The study was partially funded by the Russian Foundation for Basic Research (grant RFBR 18-29-12050-mk).

Keywords: luminescence • quantum yield • temperature • lanthanide • single crystal

References:

[1] M. S. Wrighton, D. S. Ginley and D. L. Morse, *J. Phys. Chem.* **1974**, *78*, 2229-2233.
[2] J. C. Boyer, N. J. J. Johnson and F. C. J. M. van Veggel, *Chem. Mater.* **2009**, *21*, 2010-2012.
[3] J. C. Boyer and F. C. J. M. van Veggel, *Nanoscale* **2010**, *2*, 1417-1419.
[4] C. Würth and U. Resch-Genger, *Appl. Spectrosc.* **2015**, *69*, 749-759.
[5] R. Dekker, D. J. W. Klunder, A. Borreman, M. B. J. Diemeer, K. Worhoff, A. Driessen, J. W. Stouwdam and F. C. J. M. van Veggel, *Appl. Phys. Lett* **2004**, *85*, 6104-6106.
[6] C. Wurth, M. Kaiser, S. Wilhelm, B. Grauel, T. Hirsch and U. Resch-Genger, *Nanoscale* **2017**, *9*, 4283-4294.
[7] C. T. Xu, Q. Q. Zhan, H. C. Liu, G. Somesfalean, J. Qian, S. L. He and S. Andersson-Engels, *Laser Photonics Rev.* **2013**, *7*, 663-697.
[8] C. Wurth, D. Geissler, T. Behnke, M. Kaiser and U. Resch-Genger, *Anal. Bioanal. Chem.* **2015**, *407*, 59-78.
[9] C. D. S. Brites, P. P. Lima, N. J. O. Silva, A. Millán, V. S. Amaral, F. Palacio and L. D. Carlos, *Nanoscale* **2012**, *4*, 4799-4829.
[10] C. D. S. Brites, A. Millán and L. D. Carlos in *Lanthanides in luminescent thermometry*, *Vol. 49* Eds.: J.-C. G. Bünzli and V. K. Pecharsky), Elsevier Science, B. V., Amsterdam, **2016**, pp. 339-427.
[11] M. Dramićanin, *Luminescence Thermometry: Methods, Materials, and Applications*, Elsevier, Cambridge, **2018**, p.
[12] C. D. S. Brites, S. Balabhadra and L. D. Carlos, *Adv. Opt. Mater.* **2019**, *7*, 1801239.
[13] E. C. Ximendes, W. Q. Santos, U. Rocha, U. K. Kagola, F. Sanz-Rodriguez, N. Fernandez, A. D. Gouveia-Neto, D. Bravo, A. M. Domingo, B. del Rosal, C. D. S. Brites, L. D. Carlos, D. Jaque and C. Jacinto, *Nano Lett.* **2016**, *16*, 1695-1703.
[14] Ł. Marciniak, K. Prorok, L. Francés-Soriano, J. Pérez-Prieto and A. Bednarkiewicz, *Nanoscale* **2016**, *8*, 5037-5042.
[15] A. Skripka, A. Morinvil, M. Matulionyte, T. Cheng and F. Vetrone, *Nanoscale* **2019**, *11*, 11322-11330.
[16] R. G. Geitenbeek, A. E. Nieuwelink, T. S. Jacobs, B. B. V. Salzmann, J. Goetze, A. Meijerink and B. M. Weckhuysen, *ACS Catal.* **2018**, *8*, 2397-2401.
[17] E. D. Martínez, C. D. S. Brites, L. D. Carlos, R. R. Urbano and C. Rettori, *Front. Chem.* **2019**, *7*, 83.
[18] C. D. S. Brites, E. D. Martínez, R. R. Urbano, C. Rettori and L. D. Carlos, *Front. Chem.* **2019**, *7*, 267.
[19] E. D. Martínez, C. D. S. Brites, L. D. Carlos, A. F. García-Flores, R. R. Urbano and C. Rettori, *Adv. Funct. Mater.* **2018**, *29*, 1807758.

[20] S. Balabhadra, M. L. Debasu, C. D. S. Brites, R. A. S. Ferreira and L. D. Carlos, *J. Phys. Chem. C* **2017**, *121*, 13962-13968.
[21] S. Balabhadra, M. L. Debasu, C. D. S. Brites, R. A. S. Ferreira and L. D. Carlos, *J. Lumin.* **2017**, *189*, 64-70.
[22] P. Huang, W. Zheng, S. Y. Zhou, D. T. Tu, Z. Chen, H. M. Zhu, R. F. Li, E. Ma, M. D. Huang and X. Y. Chen, *Angew. Chem. Int. Edit.* **2014**, *53*, 1252-1257.
[23] W. Zheng, P. Huang, Z. L. Gong, D. Tu, J. Xu, Q. L. Zou, R. F. Li, W. W. You, J. C. G. Bunzli and X. Y. Chen, *Nat. Commun.* **2018**, *9*, 3462.
[24] S. Kuznetsov, Y. Ermakova, V. Voronov, P. Fedorov, D. Busko, I. A. Howard, B. S. Richards and A. Turshatov, *J. Mater. Chem. C* **2018**, *6*, 598-604.
[25] S. A. Kazanskii, A. I. Ryskin, A. E. Nikiforov, A. Y. Zaharov, M. Y. Ougrumov and G. S. Shakurov, *Phys. Rev. B* **2005**, *72*, 014127
[26] D. Q. Chen, Y. L. Yu, F. Huang, P. Huang, A. P. Yang and Y. S. Wang, *J. Am. Chem. Soc.* **2010**, *132*, 9976-9978.
[27] J. Y. Sun, J. B. Xian, X. Y. Zhang and H. Y. Du, *J. Rare Earths* **2011**, *29*, 32-38.
[28] C. M. Zhang, Z. Y. Hou, R. T. Chai, Z. Y. Cheng, Z. H. Xu, C. X. Li, L. Huang and J. Lin, *J. Phys. Chem. C.* **2010**, *114*, 6928-6936.
[29] J. Y. Sun, J. B. Xian and H. Y. Du, *Appl. Surf. Sci.* **2011**, *257*, 3592-3595.
[30] M. Y. A. Yagoub, H. C. Swart, L. L. Noto, J. H. O'Connel, M. E. Lee and E. Coetsee, *J. Lumin.* **2014**, *156*, 150-156.
[31] T. Y. Glazunova, A. I. Boltalin and P. P. Fedorov, *Russ. J. Inorg. Chem.* **2006**, *51*, 983-987.
[32] Y. P. Du, X. Sun, Y. W. Zhang, Z. G. Yan, L. D. Sun and C. H. Yan, *Cryst. Growth. Des.* **2009**, *9*, 2013-2019.
[33] A. A. Luginina, P. P. Fedorov, S. V. Kuznetsov, M. N. Mayakova, V. V. Osiko, V. K. Ivanov and A. E. Baranchikov, *Inorg. Mater.* **2012**, *48*, 531-538.
[34] L. Schmidt, F. Emmerling, H. Kirmse and E. Kemnitz, *RSC Adv.* **2014**, *4*, 32-38.
[35] Y. A. Rozhnova, S. V. Kuznetsov, A. A. Luginina, V. V. Voronov, A. V. Ryabova, D. V. Pominova, R. P. Ermakov, V. A. Usachev, N. E. Kononenko, A. E. Baranchikov, V. K. Ivanov and P. P. Fedorov, *Mater. Chem. Phys.* **2016**, *172*, 150-157.
[36] P. P. Fedorov, V. B. Aleksandrov, O. S. Bondareva, I. I. Buchinskaya, M. D. Val'kovskii and B. P. Sobolev, *Crystallogr. Rep.* **2001**, *46*, 239-245.
[37] R. D. Shannon, *Acta Crystallogr A* **1976**, *32*, 751-767.
[38] H. Ishida, S. Tobita, Y. Hasegawa, R. Katoh and K. Nozaki, *Coordin. Chem. Rev.* **2010**, *254*, 2449-2458.
[39] B. P. Sobolev and K. B. Seiranian, *J. Solid State Chem.* **1981**, *39*, 337-344.
[40] S. V. Kuznetsov and P. P. Fedorov, *Inorg. Mater.* **2008**, *44*, 1434-1458.

SHORT BIO

Carlos DS Brites is Assistant Professor in the Physics Department of the University of Aveiro and member of CICECO – Aveiro Institute of Materials. He finished his Ph.D. in Physics in the MAP-FIS joint program (2012) and was hosted in CICECO/UA and ICMA (Univ. of Zaragoza, Spain). His current research interests cover luminescent materials based on trivalent lanthanide ions for thermometry and for molecular logic.

Dr. Sergey V. Kuznetsov graduated from the Lomonosov Moscow State Academy of Fine Chemical Technology in 2004. He completed his Ph.D. in Chemical Technology at the Prokhorov General Physics Institute of Russian Academy of Sciences in 2007.From 2004 to the present day, worked in Laboratory of technology of nanomaterials for photonics in the Prokhorov General Physics Institute RAS as leading researcher. His research interests included materials science, luminescence, chemistry of inorganic fluorides. He received Diploma of Russian Academy of Sciences for young scientists for preparation and investigation of fluoride laser nanoceramics (2014); Diploma of the Federal Service for Intellectual Property in the nomination “100 best patents of Russia” (2012).

Dr. Vasiliy A. Konyushkin graduated from the Moscow Power Engineering Institute in 1978. From 1978 to 1979 worked as an engineer at the Research Institute of Automatic Systems. From 1981 to the present day, worked in Lebedev Physical Institute of the USSR and General Physics Institute of the Academy of Sciences of the USSR. He completed his Ph.D. in Technical Technology at the Prokhorov General Physics Institute of Russian Academy of Sciences in 2005. Currently works in Prokhorov General Physics Institute of the Russian Academy of Sciences as a Head of the "Technologies of Fluoride Materials" Laboratory. He is specialist on crystal growth of fluoride materials.

Andrey Nakladov graduated from the Moscow Institute of Engineering and Physics in 1978. From 1984 to 2005 he worked as researcher in Plasma physics department of Prokhorov General Physics Institute of the Russian Academy of Sciences. From 2006 to the present day, he works in Laboratory of Technologies of Fluoride Materials of this institute as researcher.

Prof. Dr. Pavel P. Fedorov completed his Ph.D. in Chemical Technology at the Shubnikov Institute of Crystallography of the USSR Academy of Sciences in 1976, and Dr. Sci. in 1991. He became professor of Crystallography and Physics of Crystals in 2001. He is head of the Department of nanotechnology in Prokhorov General Physics Institute of Russian Academy of Sciences. His research interests included thermodynamics, materials science, chemistry of inorganic fluorides. He received many scientific awards, including Kuo-Mo-Jo Medal of Chinese Academy of Sciences (1988), Joint Award of the USSR and Czechoslovak Academies of Sciences (1989), Diplomas of the Federal Service for Intellectual Property in the nomination “100 best patents of Russia” (2012; 2013).

Luís D. Carlos is Full Professor in the Department of Physics at the University of Aveiro head of the Phantom-g Group and vice-director of the CICECO-Aveiro Institute of Materials (Portugal). He is member of the Lisbon Academy of Sciences and of the Brazilian Academy of Sciences. His current research interests include luminescent nanothermometers, luminescent solar concentrators, organic-inorganic hybrids for green photonics (solid-state lighting and integrated optics), and single-ion and single-molecule magnets.

Entry for the Table of Contents

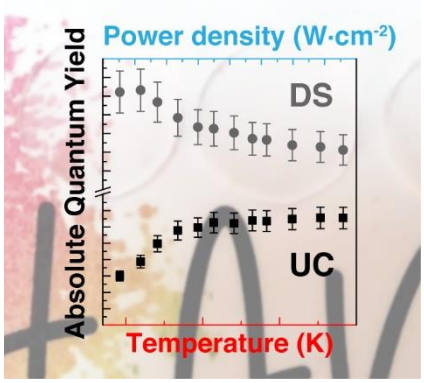

The simultaneous determination of the emission quantum yield for downshifting and upconverting processes and the temperature is reported using the output of a commercial integrating sphere. The temperature is calculated by primary luminescence thermometry through the Boltzmann equation. The procedure is illustrated using of SrF_2: Yb^{3+}/Er^{3+} single crystals.

Twitter usernames: @ciceco_ua @PhantomG_Aveiro @carlosdsbrites @LuisCarlos_zito